Ground heat exchanger performance with variable speed ground-source heat pumps

Geoffrey Viviescas   **Michel Bernier**

ABSTRACT

The objective of this paper is to compare the required length and performance of ground heat exchangers as well as heat pump energy consumption for fixed and variable speed ground-source heat pumps. In the first part of the paper, a physics-based model of a water-to-water heat pump is briefly presented. This model is incorporated in TRNSYS simulations using a performance map where variable speed operation is handled through a linear relationship linking the COP to the percentage of the full capacity being used. The ground heat exchanger is modeled using a thermal resistance and capacitance approach to account for borehole thermal capacity. Simulations are performed on a typical residential building located in a cold climate (Montréal, Canada) and equipped with either a fixed or variable speed groud-source heat pump. Results are obtained for eight cases with: variable or fixed speed operation (VSC or FSC), with or without consideration of borehole thermal capacity (TC or NTC), and with annual heating needs covered at 90% or 100% by the heat pump. The differences in the required borehole length between the TC and NTC cases are relatively small. The smallest required borehole length is for the FSC-90%-TC case (180 m) and the longest is for the VSC-100%-TC case (250 m). The VSC-100% case has the largest seasonal Performance factor (SPF) at 4.14 and the FSC-90% case has the lowest at 3.11.

INTRODUCTION

Ground-source heat pumps equipped with variable speed compressors (VSGSHP) offer the possibility of matching the building heating and cooling loads by modulating the compressor speed. This is accomplished by tuning the inlet frequency (typically down to 20-30 Hz and up to 90-120 Hz) to the electric motor of the compressor. Thus, contrary to fixed speed ground-source heat pumps (FSGSHP) which operate in on/off mode, VSGSHP operates continuously except for low load conditions. Furthermore, VSGSHP can meet a greater portion of the heating loads without requiring auxiliary heat. Thus, the ground heat exchanger (GHE) of a VSGSHP will experience loads that are different than the ones of an FSGSHP. In turn, this affects the required length and thermal performance of the GHE.

Bouheret and Bernier (2018) have reviewed the literature on variable capacity water-to-air ground-source heat pumps. They proposed an approach to model a commercially available product (ClimateMaster, 2022) that can provide heating, cooling, and domestic hot water (DHW). They showed that the annual SPF (i.e. ratio of the annual energy requirement for heating, cooling, and DHW over the annual electricity consumption) can reach 3.64. However, their analysis did not examine the impact of the variable speed operation on the GHE itself.

A residential-size ground-source integrated heat pump (GSIHP) system was developed by Rice et al. (2013). Experimental test results were used to calibrate a model in TRNSYS which was used to predict annual energy savings for five US locations. Results indicate that the GSIHP offered average savings of 55% when compared to a typical air source heat pump (ASHP). The required length of the GHE for the GSIPH was 25% higher than a ground-source heat pump equipped with a desuperheater for DHW. Except for this last article, very few studies have examined in detail the impact of the operation of a VSGSHP on the performance of GHE.

Thus, the objective of this paper is to compare the required length and performance of ground heat exchangers (GHE) as well as heat pump energy consumption for fixed and variable speed ground-source heat pumps. The paper starts with a brief description of the system being investigated. Then, the heat pump model used in the simulations is presented.

Geoffrey Viviescas (geoffrey.viviescas@polymtl.ca) is a Ph.D. candidate and Michel Bernier (michel.bernier@polymtl.ca) is a professor of mechanical engineering at Polytechnique Montreal.

164

This is followed by a presentation of the results and concluding remarks.

SYSTEM UNDER INVESTIGATION

The system under investigation is shown in Figure 1 and the characteristics of the main components are given in Table 1 along with the model (Type) used in the TRNSYS simulations. It consists of a residence located in Montréal and heated by a water-to-water heat pump coupled to a vertical GHE. Space cooling is not considered in this study and the same configuration is used for FSGSHP and VSGSHP. A thermostat activates a circulation pump that feeds a series of radiators with hot water from a buffer tank to maintain the house at 21 °C. The buffer tank provides a means to decouple the heat pump operation from the distribution loop in the building. Buffer tanks are commonly used for fixed-speed heat pumps to avoid excessive cycling. It is also possible to link a VSGSHP directly to a distribution loop given the ability to provide varying load side temperatures. However, it was decided to keep the buffer tank for the VSGSHP system considering that comparisons were to be made with FSGSHP.
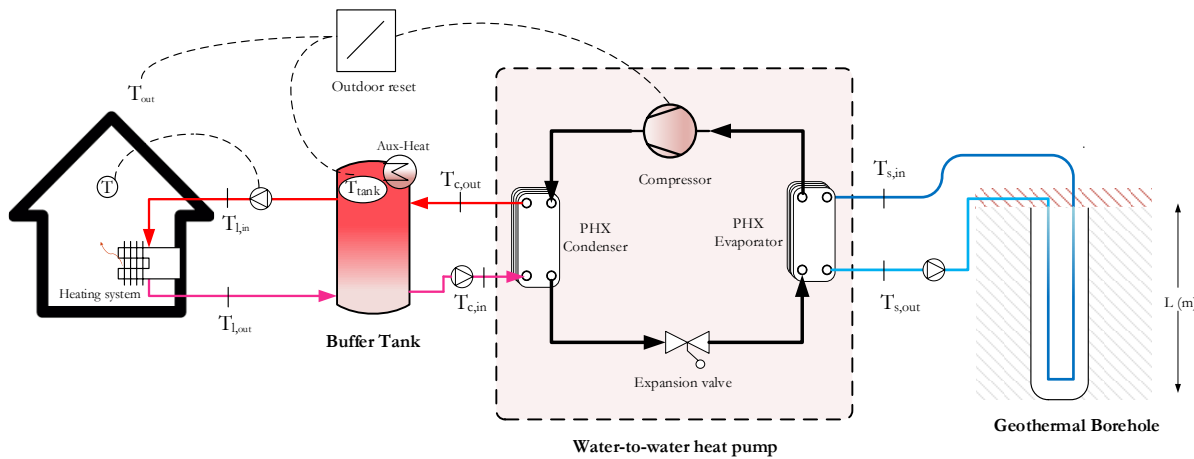

Figure 1 Schematic representation of the system under investigation

Table 1 Main components used in simulations

Component	TRNSYS TYPE	Principal characteristic	Value
Building	88	Overall building loss coefficient, UA [kW/K]	0.225
		Building mass, MCp [kJ/K]	50000
Buffer tank	158	Volume [m³]	0.5
		Height [m]	2
		Auxiliary heaters [kW]	2 x 2.5
FSGSHP	927	Performance given in Figure 4 for a fixed frequency of 60 Hz	
VSGSHP	Slightly modified version of Type 1323_v2a	Performance given in Figure 4	
Borehole	243 (in-house model developed to model borehole thermal capacity- See Godefroy et al. (2016)	Borehole radius [m]	0.075
		Ground thermal conductivity [W/m-K]	2.22
		Ground thermal capacitance [kJ/m3/K]	2000
		Grout thermal conductivity [W/m-K]	0.833
		Grout thermal capacitance [kJ/m3/K]	0 or 3900
		Pipe thermal conductivity [W/m-K]	0.416
		Borehole thermal resistance [m-K/W]	0.178

The top tank temperature is regulated by an aquastat which sends a signal to the heat pump to operate. In the case of the FSGSHP, an on/off signal is sent to the heat pump. For the VSGSHP, the compressor speed is regulated to achieve the desired outlet temperature (i.e. the top tank temperature). The top tank set point temperature, T_{set}, is adjusted using a simple outdoor reset control based on the ambient temperature, T_{out}, (T_{set} = -0.556 × T_{out} + 33.3) leading to maximum and minimum tank set point temperatures of 50 °C and 25 °C, respectively.

This enables lowering the tank temperature in mild weather to increase heat pump COP and reduce energy consumption. If the heat pump is unable to meet the tank set point temperature, two auxiliary heaters (2.5 kW each) are activated in stages when the tank temperature is 2 °C and °3 C below T_{set}. On the source side, the heat pump is connected to a ground heat exchanger (GHE) and two constant flow circulating pumps are activated whenever the heat pump is operating.

VARIABLE SPEED GROUND-SOURCE HEAT PUMP MODEL

A VSGSHP model was developed for this study and integrated in TRNSYS using a performance map. This model is part of a broader study aimed at developing a detailed physics-based and experimentally validated model of a water-to-water heat pump. Initial steps towards this goal were documented recently (Viviescas et al., 2021) and more details on this model will be presented in the near future. The following paragraphs contain only the salient features of the model that are pertinent to the present study.

The VSGSHP modeled here is equipped with two plate heat exchangers (evaporator and condenser), a variable speed compressor, and an expansion valve as shown in Figure 1. Each of these four components is modeled individually and linked together via the refrigeration cycle. Steady-state operation is assumed at each time step and pressure drops in both heat exchangers are assumed to be negligible. R-410A is used as the refrigerant. Detailed heat transfer models are used for both heat exchangers. This enables the prediction of the number of degrees of superheating and subcooling for a given refrigeration flow rate (Viviescas et al., 2021). A constant enthalpy process is assumed in the expansion valve. The compressor requires special treatment and the next paragraphs describe the approach used here.

Researchers have proposed various approaches to model variable speed compressors. For example, Shao et al. (2004) proposed a model built on second-order correlations based on condensation and evaporation temperature for the basic frequency. These correlations are then corrected with a second-order frequency correlation for other frequencies. In this work, the compressor is modeled using an extension of the approach suggested in standard CAN/ANSI/AHRI 540-2020 (AHRI, 2020). This standard proposes to fit fixed-speed experimental data into a third-order polynomial equation with 10 coefficients as shown in Equation 1 :

$$X = C_1 + C_2 T_S + C_3 T_D + C_4 T_S^2 + C_5 T_D T_S + C_6 T_D^2 + C_7 T_S^3 + C_8 T_D T_S^2 + C_9 T_S T_D^2 + C_{10} T_D^3 \qquad (1)$$

where C_1 to C_{10} are the regression coefficients, T_D is the discharge dew point temperature in °C, (i.e. condensing temperature corresponding to saturation at x=1), T_S is suction dew point temperature in °C, (i.e. evaporating temperature corresponding to saturation at x=1), and X is either the power input (in W), cooling capacity (in W), or refrigerant mass flow (kg h^{-1}).

This approach has been adapted here to include variable speed compressors by introducing frequency as a parameter. This variable is related to the speed of rotation of the compressor and therefore the mass flow rate and the power of the compressor depending on the frequency. Preliminary statistical analysis indicates that using a third order polynomial with 20 coefficients correlates both the mass flow rate and power of a variable speed compressor with good accuracy:

$$\begin{aligned} X = C_1 + C_2 T_s + C_3 T_D + C_4 f_{Hz} + C_5 T_s^2 + C_6 T_D^2 + C_7 f_{Hz}^2 + C_8 T_s f_{Hz} + C_9 T_D f_{Hz} + C_{10} T_s T_D + C_{11} T_s T_D f_{Hz} + C_{12} T_s^2 T_D \\ + C_{13} T_D^2 T_s + C_{14} T_s^2 f_{Hz} + C_{15} f_{Hz}^2 T_s + C_{16} T_D^2 f_{Hz} + C_{17} f_{Hz}^2 T_D + + C_{18} T_s^3 + C_{19} T_D^3 + C_{20} f_{Hz}^3 \end{aligned} \qquad (2)$$

where f_{Hz} is the frequency in Hz.

The compressor power and refrigerant mass flow rate given by equation 2 were coupled to the rest of the components of the model resulting in a set of nonlinear equations. The solution of this set of equations gives the heating capacity (at the condenser) and the COP which is simply the ratio between the capacity and the power given by Equation 2. A commercially available scroll compressor (Danfoss VSH088-G) was chosen for this study. The estimation of the coefficients was carried out using the STATISTICA® software using multiple linear regression. The resulting coefficients are presented in Table 2.

The values of these coefficients are specific to this compressor. Modeling of other compressors that differ in size and design is planned in a further study.

Figure 2 shows a comparison between the experimental results and the 20-coefficient equation for the power input. It can be seen that the agreement between the 20-coefficient equation and experimental results is very good. The mean and maximum differences are 0.8 % and 3.5 % over the full range of conditions (similar results were obtained for the mass flow rate). It should be noted that the resulting degrees of superheating or subcooling did not always correspond exactly to the values associated with Equation 2. In these cases, the equation contained in Appendix D of the standard (AHRI, 2020) was used to adjust mass flow rates for various degrees of superheat by using the change in refrigerant density at the suction of the compressor.

The original plan was to develop a TRNSYS type with its own internal solver that could perform such calculations at each time step in a simulation. However, this proved to be difficult due to convergence issues associated with the correct choice of guess values to solve the set of nonlinear equations. Instead, individual component models were implemented and linked together in the Engineering Equation Solver (EES, 2022) software tool where guess values could be changed more easily. The integrated models were solved by changing the frequency (from 30 to 90 Hz in increments of 10 Hz) and the inlet temperatures of both secondary fluids (from -2 to 10 °C in increments of 2 °C for the source side and from 30 to 50 °C in increments of 5 °C on the load side. For this study, the flow rates of the secondary fluids were kept constant (at 0.5 kg/s) to limit the number of independent variables.

| Table 2 Input coefficients to equation 2					
	Power [W]	Mass-flow [kg/h]		Power [W]	Mass-flow [kg/h]
C1	-2200.6	-12.80	C11	0.0067	0.00029
C2	-55.6	-0.4251	C12	0.0275	-0.00036
C3	151.6	-0.2964	C13	-0.0175	-0.00043
C4	79.8	8.4103	C14	0.0059	0.00354
C5	-1.612	0.0189	C15	0.0006	0.00002
C6	-3.923	-0.01016	C16	-0.0058	-0.00026
C7	-0.4734	-0.00058	C17	0.01828	-0.00014
C8	0.2950	0.28141	C18	-0.0067	0.00154
C9	0.5560	0.03704	C19	0.0451	-0.00001
C10	1.5683	0.01319	C20	-0.00032	-0.00001
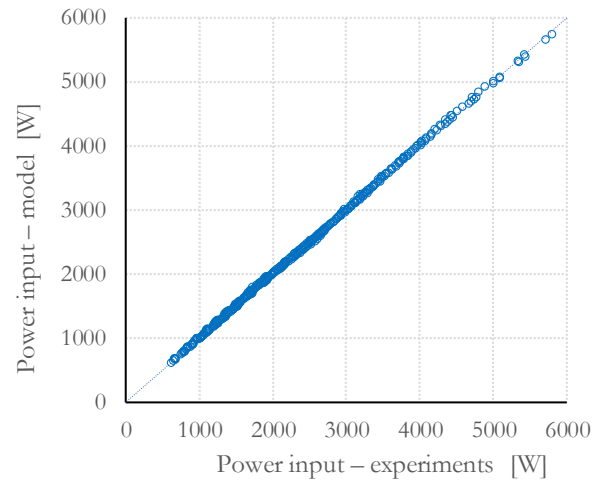
Figure 2 Comparison of the 20-coefficient model with manufacturer data.

It is interesting to examine the performance of the VSGSHP for several conditions. Figure 3 shows the normalized heating capacity for three combinations of $T_{s,in}/T_{c,in}$ and seven frequencies. As expected, the COP increases as the temperature difference between the source and load temperatures decreases. For a given $T_{s,in}/T_{c,in}$ combination the COP reaches a peak value at different frequencies. For example, for the 5°C /35°C combination, the COP is maximum at 50 Hz and it decreases when the frequency is either increased or decreased. As expected, the heating capacity increases with frequency as the refrigerant flow rate increases.
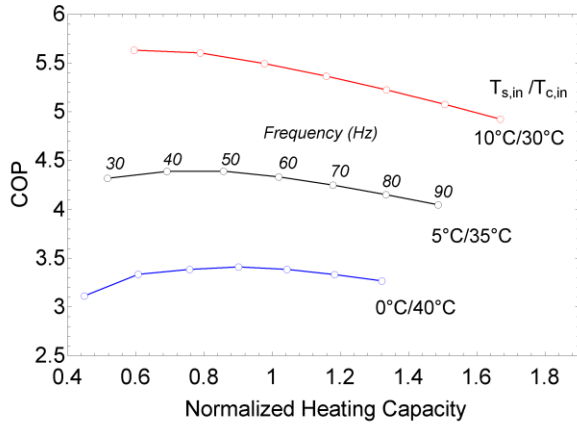
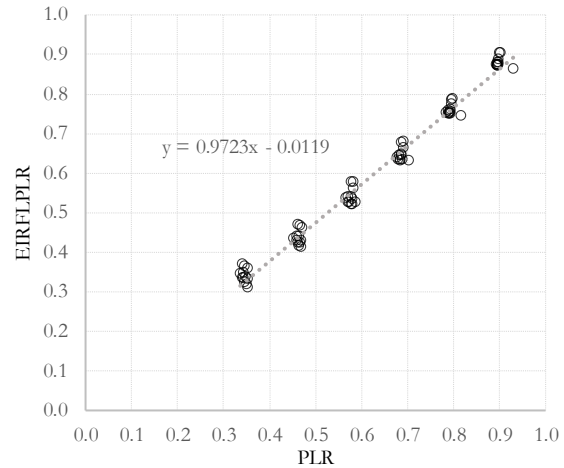Figure 3 Normalized heating capacity for the VSGSHP

Figure 4 Part load performance of the VSGSHP

The full set of data was split in two: Data at full load (90 Hz) and data at partial load (from 30 to 80 Hz). Figure 5 shows the first few lines of the performance map at full load. Data were normalized at 5°C on the source side and 35°C on the load side.

```
30       35       40       45       50       !Entering Load Temperatures (C)
-2       0        2        4        6        8        10        !Entering Source Temperatures (C)
0.855    0.896                      !Normalized Heat Capacity, normalized power at 90Hz, 30[°C],-2[°C]
0.898    0.902                      !Normalized Heat Capacity, normalized power at 90Hz, 30[°C], 0[°C]
0.944    0.908                      !Normalized Heat Capacity, normalized power at 90Hz, 30[°C], 2[°C]
```

Figure 5 Excerpt of the performance map of the VSGSHP at full load (90 Hz)

To account for operation at other frequencies (i.e. at part load), the approach implemented in TRNSYS Type 1323_v2a (variable speed heat pump model) is used. The energy input ratio as a function of temperature (EIRFPLR) is calculated as a function of the ratio of the actual capacity to the full load capacity (also known as the Part Load Ratio, PLR) for the same source and load inlet temperatures. Using the second set of data it was then possible to establish a correlation between EIRFPLR and PLR. As shown in Figure 4 a linear relationship was found to fit the data with relatively good accuracy. Also, since compressor operation below 30 Hz is not recommended, the curve stops at a PLR ~ 0.35. Thus, whenever a PLR of 0.35 is reached, the VSGSHP stops and cycles to meet the set point temperature. The original TRNSYS Type 1323_v2a was modified to account for cycling operation below 30 Hz.

The FSGSHP was modeled in TRNSYS using Type 927 which also uses a performance map. To make a fair comparison between the VSGSHP and the FSGSHP, the same compressor was used for the FSGSHP but with a fixed operating frequency of 60 Hz.

Heat pump cycling losses for either the FSGSHP or the VSGSHP (below 30 Hz) are handled using the approach proposed by Fuentes et al. (2016) which is based on an experimental study carried out to characterize the behavior of water-to-water heat pumps that operate under partial load. Start-up (C_d) and degradation (C_c) coefficients equal to 0.22 and 0.998 are used.

RESULTS AND DISCUSSION

Simulations are performed over 10 years with a 6-minute time step. The required borehole length is determined on a trial and error basis, where the length is varied until the minimum inlet temperature to the heat pump reaches a value of 0 °C. Of interest are the required length of the borehole, the annual energy consumption, the coefficient of performance COP, and the seasonal performance factor (SPF).

Various scenarios are explored to cover the following three effects: Variable or fixed speed operation (VSC or FSC),

with or without (TC or NTC) consideration of borehole thermal capacity, and the proportion of the annual heating needs (90% or 100%) covered by the heat pump. The cases are identified with an acronym such as VSC-100%-TC. A total of eight cases are presented to cover the various combinations. In terms of the proportion of the annual heating needs being covered by the heat pump, it was decided to examine two cases where 90% and 100% of the annual heating needs are covered by the heat pump. In other words, in the first case, auxiliary heat provides 10% of the annual heating load (typically at peak load conditions) while in the second case auxiliary heat is not required.

Global annual results are shown in Table 3 for the eight cases while Table 4 presents the peak load on the borehole, q_h, as well as the monthly (q_m) and yearly (q_y) average loads, values which are typically used in borehole sizing (Philippe et al. 2010). The peak borehole load is particularly important and might be responsible for up to 50 to 80% of the required length. As shown in Table 3, the rated heating capacity is substantially higher when 100% of the annual needs are covered. For example, for the VSC-TC cases, the rated heating capacities are 9.51 kW and 5.69 kW for the 100% and 90% cases, respectively. This has a substantial impact on the peak borehole load. As shown in Table 4 for the same two cases, the peak hourly loads are 6.36 kW and 4.54 kW, respectively. The monthly ground loads during the peak month are also quite different (4.80 vs 4.17 kW) as well as the yearly ground load (2.29 vs 2.15 kW).

Table 3. Rated heating capacity and power as well as various annual energy values

Parameter	Units	VCS-100% TC	VCS-100% NTC	VSC-90% TC	VSC-90% NTC	FSC-100% TC	FSC-100% NTC	FSC-90% TC	FSC-90% NTC
Rated Heating Capacity	[kW]	9.51	9.51	5.69	5.69	9.87	9.87	5.56	5.56
Rated Heating Power	[kW]	2.36	2.36	1.41	1.41	2.36	2.36	1.33	1.33
Heating needs by HP	[kWh/y]	26354	26353	23879	23870	26317	26317	23757	23706
Bore energy extracted	[kWh/y]	20129	20125	18195	18186	20021	20021	18073	18015
Compressor energy	[kWh/y]	6225	6229	5684	5685	6297	6297	5684	5690
Auxiliary Energy	[kWh/y]	33	35	2324	2330	0	0	2310	2316
% Auxiliary heating	%	0.12	0.13	9.73	9.76	0.00	0.00	9.72	9.77

Table 4. Hourly, monthly and annual max loads on the borehole for the 8 cases

Parameter		VCS-100% TC	VCS-100% NTC	VSC-90% TC	VSC-90% NTC	FSC-100% TC	FSC-100% NTC	FSC-90% TC	FSC-90% NTC
Peak hourly mean ground load [kW]	q_h	6.36	6.53	4.54	4.81	6.53	6.65	4.15	4.36
Monthly mean ground load [kW]	q_m	4.80	4.84	4.17	4.20	4.87	4.89	3.94	3.96
Yearly mean ground load [kW]	q_y	2.29	2.29	2.15	2.15	2.29	2.28	2.06	2.06

The required borehole length for each case is shown in Figure 6. The first point to note is that there is not a large difference in the required borehole length when borehole thermal capacity is included in the borehole model. One would have expected the FSC cases to show greater differences between the TC and NTC cases since cycling should enable the borehole thermal capacity to dampen the peak loads (Gagné-Boisvert and Bernier, 2016). However, peak conditions for the FSC cases last for several hours which eliminates the beneficial effect of borehole thermal capacity. For the VSC cases, the heat pump capacity is adjusted at every time step and the borehole load changes accordingly, and these changes are dampened by borehole thermal capacity. This can be seen in Figure 7 where the borehole load and outlet temperature variations at peak conditions are shown for one week in the middle of January. The borehole load variation is smoother when borehole thermal capacity is included. As shown in Figure 7, this leads to a slightly lower required borehole length when TC is included. Since the differences in results between TC and NTC cases are small, only TC results will now be compared. As shown in Figure 6, the minimum required length is for the FSC-90% cases at 180 m while the maximum length is for the FSC-100% cases at 255 m, a difference of about 40%. This difference is simply because values of q_h, q_m, and q_y are all higher for the FSC-100% case as shown in Table 4. The same reasoning applies when the VSC-100% and the VSC-90% cases are compared.
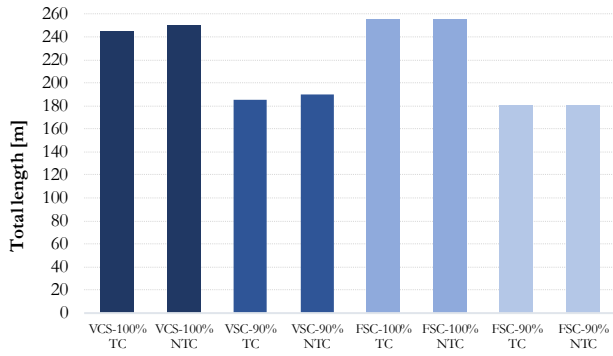
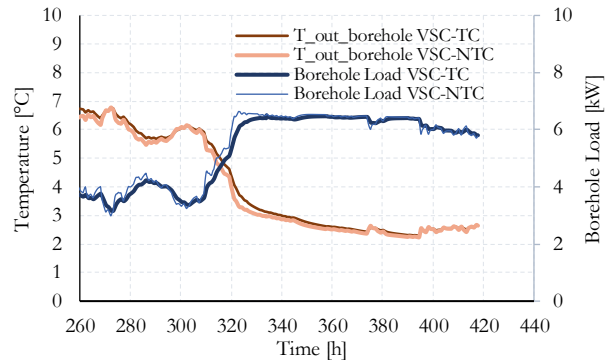Figure 6 Required borehole length for the eight cases

Figure 7 VSC-100% (TC-NTC) cases during peak conditions

When the annual heating load is met entirely by the heat pump including at peak conditions (FSC-100%-TC and VSC-100%-TC) it is interesting to note that the VSC has a lower required borehole length (245 m) when compared to the FSC case (255 m), a difference of 4%. This difference is explained by different values of q_h, q_m, and q_y as shown in Table 4. The higher value of q_h is because at peak load (approximately represented by the 0°C/40°C curve in Figure 3) the COP is higher at 60 Hz (for the FSGSHP) than at 90 Hz (for the VSGSHP operating at the maximum frequency). A higher COP implies that the borehole load is higher for the same load. Figure 8a shows the variation of the top tank temperature, outlet borehole temperature, and borehole load around the peak conditions. For t < 320 h, the cycling of the FSC can be seen. For 320 < t < 400 h, at peak conditions, the FSC operates continuously. After t >400 h cyclic operation is also shown. In contrast, the VCS shows much smoother variations of the top tank temperature, outlet borehole temperature, and borehole load throughout this time interval.

The situation is reversed when 90% of the annual heating load is met by the heat pump: the VSC has a higher required length (185 m) than the FSC (180 m), a 3 % difference. Here the difference is attributable to the heat pump capacity at peak conditions. Even though care was taken to obtain the same amount of auxiliary energy on an annual basis (10%), results in Table 4 reveal that the annual amount of auxiliary heat is 9.73 and 9.76 % for the VSC and FSC, respectively. Thus, the VSC requires slightly more heat from the borehole. Furthermore, the VSC and FSC have different COP (Figure 3). These two factors lead to different values of q_h at peak conditions, 4.54 kW for the VSC case and 4.15 kW for the FSC case, which explains the difference in the borehole length.

Figure 8b shows a comparison between the VSC-100% and FSC-90% cases around peak conditions. As was observed in Figure 8a, the cycling nature of the FSC can be seen. In addition, the operation of the two auxiliary heaters is shown with the first stage at 2.5 kW and the two stages at 5 kW. The borehole load at the peak conditions is a little below 4 kW for the FSC case while it is slightly above 6 kW for the VSC case.
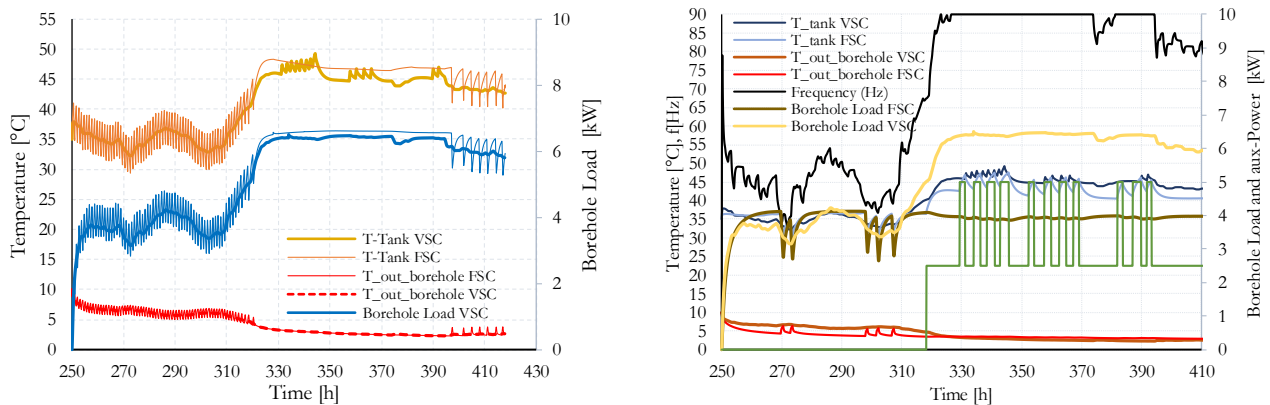

Figure 8 System behaviour a) VSC100% vs FSC100%; b) VSC-100% vs FSC90%

170

The black line in figure 8b shows the compressor frequency during the period of highest thermal load. For t < 320 h, the VSC works at reduced speeds operating at frequencies between 30-90 Hz. For 320 < t < 370 h, at peak conditions, the VSC operates continuously at full capacity (90Hz).

Another metric for comparison is the seasonal performance factor (SPF) which is defined here using:

$$SPF = \frac{\sum_{j=1}^{n} Q_{Load,j}}{\sum_{j=1}^{n}(W_{net,j} + W_{aux,j})} \tag{3}$$

where n is the number of times steps during the heating season, $Q_{load,j}$ is the amount of energy required to heat the building, $W_{net,j}$ is the amount of energy required by the compressor and $W_{aux,j}$ is the amount of auxiliary heating plus the amount of energy associated with cyclic losses. SPF values for four cases are shown in Figure 9.

The VSC-100% case has a higher SPF (4.14) than the FSC-100% case (4.01). Since there is no auxiliary heating, in either case, the difference is due to a combination of higher COP for the VSC-100% case and higher cycling losses for the FSC-100% case. The VSC-90% case has also a higher SPF than the FSC-90% case (3.25 vs 3.11). Aside from the higher cycling losses associated with the FSC case, two other reasons explain this difference. First, the nominal capacity of the VSC is slightly higher than that of the FSC (see Table 3), reducing the use of auxiliary heating (9.73% compared to 9.76% for the FSC). Secondly, the temperature difference between the source and the load (borehole and tank) oscillates less in the VSC leading to less oscillation in the value of the temperatures and better COPs.
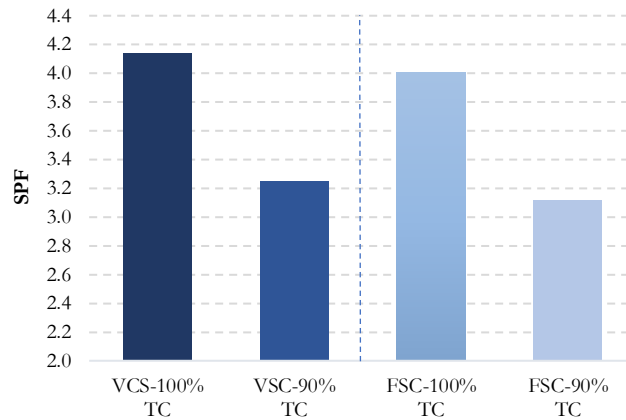

Figure 9 Seasonal performance factor (SPF) for four cases

CONCLUSION

The required length and thermal performance of ground heat exchangers, as well the heat pump energy consumption for fixed and variable speed ground-source heat pumps, are investigated in this study. In the first part of the paper, the fixed and variable speed ground-source heat pump models are described. The compressors are modeled using third-order correlations with 20 coefficients obtained by adapting the standardized procedure of the AHRI 540-2020 standard. The global model is assembled in the EES software tool to solve the system of nonlinear equations. This information is used to develop a performance map along with a modified version of TRNSYS Type1323_v2a used to model variable speed water-to-water heat pumps. Ten-year simulations of a residence located in Montréal are performed with a six-minute time step.

In the results section, various scenarios are explored to cover the following three effects: Variable or fixed speed operation (VSC or FSC), with or without (TC or NTC) consideration of borehole thermal capacity, and with annual heating needs covered at 90% or 100% by the heat pump. The differences in the required borehole length between the

TC and NTC cases are relatively small in the present case probably because the residential building has a long and almost constant peak period which reduces the beneficial effect of borehole thermal capacity. The smallest required length is for the FSC-90%-TC case (180 m) and the longest is for the VSC-100%-TC case (250 m). This represents a 40% difference. The VSC-100% case has the largest SPF at 4.14 and the FSC-90% case has the lowest SPF at 3.11. This is due to the negligible use of auxiliary heating and the reduction in heat pump cycling losses for the VSC-100% case. A comparison between the VSC-100% and the FSC-100% cases, thus with no auxiliary heating, indicates that variable speed operation leads to a better SPF (4.14 vs 4.01) and to a 3.2% reduction in annual energy consumption.

Cooling-dominated or balanced systems were not considered in this study. For cooling-dominated systems, the higher COP of the VSC would most likely lead to shorter boreholes. As for balanced systems, it is difficult to predict whether the FSC or the VSC would lead to shorter boreholes without doing further studies. Furthermore, pumping energy on both the source and load sides should also be considered. The conclusions obtained here are specific to the present case. Different climates, buildings, and types of compressors need to be examined to generalize the conclusions.

NOMENCLATURE

T_{out} = room temperature (°C)

T_{set} = tank temperature set point (°C)

$T_{s,in}$ = temperature out from the borehole (°C)

$T_{c,in}$ = temperature out tank to heat pump(°C)

Subscripts

c = condenser

s = source

REFERENCES

AHRI. 2020. National standard CAN/ANSI/AHRI 540-2020 Performance Rating of Positive Displacement Refrigerant Compressors.

ASHRAE. 2015. Chapter 34 Geothermal energy. ASHRAE Handbook, HVAC applications, Atlanta, GA:.

Bouheret, S. and M. Bernier. 2018. *Modelling of a water-to-air variable capacity ground-source heat pump*. Journal of Building Performance Simulation, 11(3), 283-293.

Climatemaster. 2022, Trilogy-45. [Online] Available at: https://www.climatemaster.com/homeowner/news/climatemaster/climatemaster/trilogy-45 [Accessed 21 March 2022].

Danfoss, 2022. VSH088 model. [Online] Available at: https://www.manualslib.com/manual/1966573/Danfoss-Vsh088.html?page=12#manual

Engineering Equation Solver (EES). 2022. F-chart software, Madison, Wiscosin, v11.365.

Enertech, 2018. WV models water-to-water heat pumps – Installation & Operations Manual. [Online] Available at: https://geocomfort.com/residential-products/item/guide-wv [Accessed 11 May 2022].

Fuentes, E., D.A. Waddicor and J. Salom. (2016). *Improvements in the characterization of the efficiency degradation of water-to-water heat pumps under cyclic conditions*, Applied Energy, 179: 778-89.

Gagné-Boisvert L. and M. Bernier. 2016. *Accounting for borehole thermal capacity when designing vertical geothermal heat exchangers*. ASHRAE summer conference, St-Louis, Missouri, June 2016. Paper ST-16-C027.

Godefroy, V., C. Lecomte, M. Bernier, M. Douglas and M. Armstrong. 2016. *Experimental validation of a thermal resistance and capacity model for geothermal boreholes*. ASHRAE winter conference, Orlando, Florida, January 2016. Paper OR-16-C047.

Philippe, M., M. Bernier and D. Marchio. 2010. *Sizing Calculation Spreadsheet:Vertical Geothermal Borefields*. ASHRAE Journal, 52(7), 20-28.

Rice, K., V. Baxter, S. Hern, T. McDonwell, J. Munk and B. Shen. 2013. *Development of a residential ground-source integrated heat pump*. ASHRAE Transactions, 119(1).

Shao, S., S. Wenxing, X. Li and H. Chen. 2004. *Performance representation of variable-speed compressor for inverter air conditionners based on experimental data*. International Journal of Refrigeration, 27(8): 805-815.

Viviescas, G., S. Houaida, M. Bernier and M. Kummert. 2021. *Energy performance advantages of using multiple compressors in a heat pump operating in heating mode*. IBPSA-Canada, eSim 2021 Conference. [Online] Available at: http://www.ibpsa.org/proceedings/eSimPapers/2021/Contribution_1211_final_a.pdf [Accessed 11 May 2022].